PCCP

Accepted Manuscript

ROYAL SOCIETY OF CHEMISTRY

www.rsc.org/pccp

Journal Name

RSCPublishing

ARTICLE

Coherent Phonon Decay and the Boron Isotope Effect for MgB_2

Cite this: DOI: 10.1039/x0xx00000x

Jose A. Alarco[*a,b], Peter C. Talbot[a,b] and Ian D. R. Mackinnon[a]

Received ooth January 2012,
Accepted ooth January 2012

DOI: 10.1039/x0xx00000x

www.rsc.org/

Ab-initio DFT calculations for the phonon dispersion (PD) and the Phonon Density Of States (PDOS) of the two isotopic forms (^{10}B and ^{11}B) of MgB_2 demonstrate that use of a reduced symmetry super-lattice provides an improved approximation to the dynamical, phonon-distorted P6/mmm crystal structure. Construction of phonon frequency plots using calculated values for these isotopic forms gives linear trends with integer multiples of a base frequency that change in slope in a manner consistent with the isotope effect (IE). Spectral parameters inferred from this method are similar to that determined experimentally for the pure isotopic forms of MgB_2. Comparison with AlB_2 demonstrates that a coherent phonon decay down to acoustic modes is not possible for this metal. Coherent acoustic phonon decay may be an important contributor to superconductivity for MgB_2.

1. Introduction

The electron-phonon interaction (EPI) and its verification through the isotope effect (IE) have played important roles in the validation of superconductivity since Fröhlich suggested the idea and a theory in 1950[1-3]. The theory arose at about the same time as experimental confirmation by Maxwell[4] and Reynolds et al.[5, 6] using Hg. This effect gained further relevance after subsequent incorporation of EPI in the BCS theory of superconductivity[7-9]. Since then, the IE has been used to establish whether the EPI is a dominant interaction in superconductors[10, 11] or whether it is a first indication of the BCS mechanism[12, 13].

As summarized by Knigavko and Marsiglio[14], the balance of two isotope effects largely determines the IE coefficient. On the one hand, increasing the phonon frequency by reducing the ionic mass serves to increase the superconducting transition temperature (T_c,) because the energy scale that governs T_c is the phonon energy. On the other hand, this mechanism also normally brings the phonon and coulomb energies closer together, thus reducing the T_c.

For MgB_2, the IE on T_c has been experimentally determined for the boron isotopes by Bud'ko et al.[15] and later extended to both boron and magnesium isotopes by Hinks et al.[16]. Both studies show a difference in T_c of ~1 K for isotopically pure end member MgB_2 compounds[16]. Hinks et al.[16] also show that the Mg isotope effect, while present, is small. Simonelli et al.[17] investigated the IE on phonon spectra of $Mg_{1-x}Al_xB_2$, including pure MgB_2 ($0 \leq x \leq 0.57$), using Raman spectroscopy. They focused on the $\mathbf{E_{2g}}$ phonon mode and determined a difference in Raman shift for the two isotopic forms of MgB_2 (see Figure 3a of reference[17]).

Raman, Infrared (IR), Inelastic X-ray and Neutron Scattering provide phonon information that may reflect the EPI and superconducting energy gaps[18-23]. Raman and IR investigation of the phonon modes of MgB_2 note the presence of additional peaks at lower frequencies[17-21, 23]. In our recent work[22], we have also observed additional Raman and IR frequencies, that do not comply with those predicted by P6/mmm group symmetry. To explain these additional signals, we have investigated reduced symmetry configurations using Density Functional Theory (DFT). These calculations show that additional Raman and IR peaks for MgB_2 can be explained by super-lattice modes that approximate a dynamic, phonon-distorted crystal structure[22]. In addition, this work identifies a correspondence of phonon energies to superconducting energy gaps, suggesting that coherent phonon decay modes, and phonon excitation from the $\mathbf{E_{2g}}$ mode, are important mechanisms for superconductivity in this structure type.

To further evaluate this model, we have used *ab-initio* DFT to calculate the phonon dispersion (PD) and the Phonon Density Of States (PDOS) of the two boron isotopic forms (^{10}B and ^{11}B) of MgB_2 based on well-determined crystallographic data using neutron and X-ray diffraction[24-26]. In addition, these calculations are compared with similar PD and PDOS models for AlB_2 under the same computational conditions. The prototype structure for MgB_2 is that of AlB_2 which shows electronic properties of a metal[27]. Details of electronic band structure, PD and PDOS for AlB_2 are well described in the literature[27-34].

2. Modeling Calculations

DFT calculations are undertaken using the CASTEP module of Materials Studio 7.0, which provides the functionality to calculate vibrational properties for a wide range of materials[35-37]. Both linear response (also known as density functional perturbation theory, DFPT) and finite displacement (FD) methods are available. Conditions for best PD results have been previously investigated and reported[22].

Based on our previous work[22], the linear response within the Local Density Approximation (LDA) with a dense k-grid (mostly customized to k = 0.02 A^{-1}) is used for this work. For the cut-off energy, CASTEP default values are initially used in calculations. However, when a default cut-off is lower than the default value for another compound within a comparison set, the cut-off is increased towards the matched value in order to check accuracy. If results from this comparison do change significantly, their dependence on the cut-off energy is further investigated, but not otherwise.

The majority of calculations are undertaken using Materials Studio 7.0 via the Microsoft Windows mode of a 12core Mac Pro Xeon 64bit workstation. This workstation operates with an Intel chip and mimics up to 24 cores. When memory requirements exceed the capacity of this computer, calculations are undertaken via the High Performance Computing (HPC) facility at QUT using multiples of 16 cores. The optimum choice for calculations on the HPC facility is 64 cores.

For unit cell calculations on MgB_2 and AlB_2 with P6/mmm symmetry, the lattice parameters $a = b = 0.3085$ nm and $c = 0.3523$ nm[24-26] and $a = b = 0.301$ nm and $c = 0.324$ nm[33, 34], respectively, are used as input values. For super-lattice unit cell calculations, appropriate multiples of these parameters are used.

3. Modeling Results

Earlier work[22] explored a range of modelled conditions for MgB_2 to evaluate the potential impact of reduced symmetry on phonon dispersion and to compare with observed frequencies via Raman and IR activity. Of the ten lower symmetry space groups evaluated, 2x super-lattice groups (that is, groups that required doubling of the unit cell in the *c*-direction) such as P-3c1 and P63mc, provide phonon dispersion model(s) consistent with experimental data and calculated vibration modes that reflect the dynamic nature of the structure particularly near the superconducting transition. Consequently, the results below address calculations for the conventional space group P6/mmm (Space Group 191) and, for comparison, the super-lattice space group P63mc (Space Group 188).

3.1 Phonon Models

A comparison of phonon frequencies for MgB_2, calculated for the individual isotopes ^{10}B and ^{11}B and their natural abundance mixture is shown Table 1. These calculations are for the generally accepted P6/mmm symmetry and the P63mc symmetry[22]. The default value of the cut-off energy for MgB_2, at the customized k-grid = 0.02 A^{-1}, is 990 eV. This value controls the number of plane waves used in the calculation and convergence of energy variations. Due to significant computational cost, the cut-off energy is balanced against grid density.

The output lattice parameters for MgB_2, after geometry optimization under these conditions, are $a = b = 0.3085$ nm and $c = 0.3523$ nm and $a = b = 0.304$ nm and $c = 0.698$ nm, for the conventional cell and the 2x super-lattice cell, respectively. These latter values indicate that the super-lattice tends to converge to smaller lattice parameters upon optimisation.

Table 2 lists the frequencies for AlB_2, calculated for the same symmetries used in Table 1 at two different cut-off energies. These energies, the default cut-off energy at 440 eV and the value at 990 eV, have been chosen to match the default values used for the MgB_2 calculations. The output lattice parameters for AlB_2, after geometry optimization under these conditions and cutoff energy 440 eV, are $a = b = 0.298$ nm and $c = 0.326$ nm and $a = b = 0.298$ nm and $c = 0.6508$ nm, for the conventional and the 2x super-lattice cell, respectively. For cutoff energies 990 eV and 720 eV, for the P6/mmm and the P63mc symmetries, respectively, the output lattice parameters for AlB_2 are exactly the same.

Figure 1 displays the calculated PDs and PDOS for different isotopic forms and imposed symmetry on MgB_2. Note the significant difference in phonon dispersion curves in the **K-G** and **G-M** reciprocal directions for the isotopic end member forms with P63mc symmetry (Figures 1b and 1c) and natural isotope form of MgB_2 (Figure 1a). In the latter, the typical "mexican hat" configuration occurs[22] at ~600 cm^{-1} while more complex dispersion curves occur for isotope end members with reduced symmetry at that frequency and at lower values.

In contrast, Figure 2 displays the calculated PDs and PDOS for the two different imposed symmetries on AlB_2. As anticipated, the PDs for AlB_2 are significantly different to MgB_2 – particularly at the 500 cm^{-1} to 700 cm^{-1} range. This difference is attributed to a shift of the $\mathbf{E_{2g}}$ mode to higher frequencies (~960 cm^{-1}) and of the $\mathbf{B_{1g}}$ mode to lower frequency (~502 cm^{-1}) for AlB_2.

3.2 Linear Trends for Calculated Phonon Frequencies

Figure 3 shows a plot of the calculated frequencies for the 2x super-lattice with P63mc symmetry using the calculated spectral values for each MgB_2 structure type shown in Table 1. In each case, the assumed low energy peak is at a similar frequency to that observed experimentally as shown in a number of publications[18-22]. The linear trendline shown in Figure 3a plots integer multiples of frequency values from the calculated vibration modes and, using the slope of the trendline, allows an estimate for a lower energy of ~114.4 cm^{-1} for an isotopically pure form of $Mg^{10}B_2$. Similar constructs for $Mg^{10/11}B_2$ and $Mg^{11}B_2$ are shown in Figures 3b and 3c and

Table 1: Calculated phonon frequencies for MgB_2 with different B isotopes

MgB_2 Phonon Mode	Frequency [cm^{-1}]					
	^{10}B		$^{10/11}B_{nat}$		^{11}B	
	P6/mmm	P63mc	P6/mmm	P63mc	P6/mmm	P63mc
	SG 191	SG 188	SG 191	SG 188	SG 191	SG 188
	-	233.4 (d)	-	233.6 (d)	-	233.4 (d)
	-	246.5 (d)	-	237.1 (d)	-	235.1 (d)
	-	326.1	-	326.1	-	326.0
E_{1u}	350.8 (d)	350.3 (d)	343.8 (d)	343.0 (d)	342.0 (d)	341.4 (d)
	-	410.4	-	394.8	-	391.3
A_{2u}	425.7	425.3	416.7	416.4	414.9	414.5
	-	537.0 (d)	-	516.5 (d)	-	512.1 (d)
E_{2g}	601.1 (d)	592.5 (d)	582.3 (d)	569.9 (d)	573.1 (d)	565.0 (d)
	-	679.5	-	653.5	-	647.9
B_{1g}	739.4	739.5	711.6	711.3	705.0	705.1

* The P63mc symmetry is a 2x super-lattice symmetry discussed in[22].

** Modes above A_{2u} show a more pronounced isotopic effect. (d) represents a degenerate frequency.

Table 2: Calculated phonon frequencies for AlB_2 with different symmetries and cutoff energies

AlB_2 Phonon Mode	Frequency [cm^{-1}]				
	Cut-off energy*		Cut-off energy*		
	440 eV		990 eV	720 eV	990 eV
	P6/mmm	P63mc	P6/mmm	P63mc	
	SG 191	SG 188	SG 191	SG 188	
	-	158.7 (d)	-	167.8 (d)	170.2 (d)
	-	160.4 (d)	-	171.3 (d)	174.8 (d)
E_{1u}	264.3 (d)	264.2 (d)	280.2 (d)	276.8 (d)	280.2 (d)
A_{2u}	405.4	405.3	424.5	420.7	424.5
	-	426.1	-	434.3	437.0
	-	454.8	-	462.6	464.2
B_{1g}	502.8	502.7	519.1	516.1	519.0
	-	544.5	-	554.8	557.4
E_{2g}	961.5 (d)	961.5 (d)	963.9 (d)	965.0 (d)	963.8 (d)
	-	997.7 (d)	-	1001.2 (d)	1000.1 (d)

*The frequencies, particularly at lower energy modes (below E_{2g}), change with the value of energy cutoff.

allow an estimate of the lower energies as 109.7cm^{-1} and 108.6 cm^{-1}, respectively.

In keeping with the fundamental assumption that a solid crystal shows three acoustic vibrational modes at **q**=0 with a frequency, ω=0, the plots in Figures 3 and 4 also show the point (0,0)[38-40]. The trendline for these plots is not constrained to (0,0) but this point is included in the determination of slope and intercept for the trend. Thus, trends in Figures 3 and 4 intercept at non-zero values while the slope of each line provides the value for a lowest vibrational mode for the super-lattice. Given potential errors in both computational and experimental models for these systems (see 4.2 below for details), there is some uncertainty of determination. For example, computational procedures require breaking the translational symmetry of plane waves, which sometimes causes deviations from the acoustic sum rule[38]. This unavoidable procedure may partially influence small deviations around the origin. Alternatively, uncertainties in the zero-point energy determination[39, 40] may also influence these values.

A consistent approach to description of phonon decay mechanisms requires an appreciation of all vibration modes at multiples of the lowest frequency as well as an allowance for effects on computed absolute values. For example, the slope of trend lines in Figures 3 and 4 is a better indicator of the average frequency behaviour, since individual (computed) frequencies are more susceptible to temperature and other effects, which may result in broadening of energy levels, and may be evident in experimental data by full-width at half maxima values (FWHM) and, in computational models, by smearing[41].

In addition, as shown in Tables 1 and 2, individual computed frequency values are influenced by the cut-off energy selection. In our earlier work[22], we grouped the phonon calculation results for MgB_2 into two separate sets of values, resulting in a slope value that is similar to the lowest frequency. Given

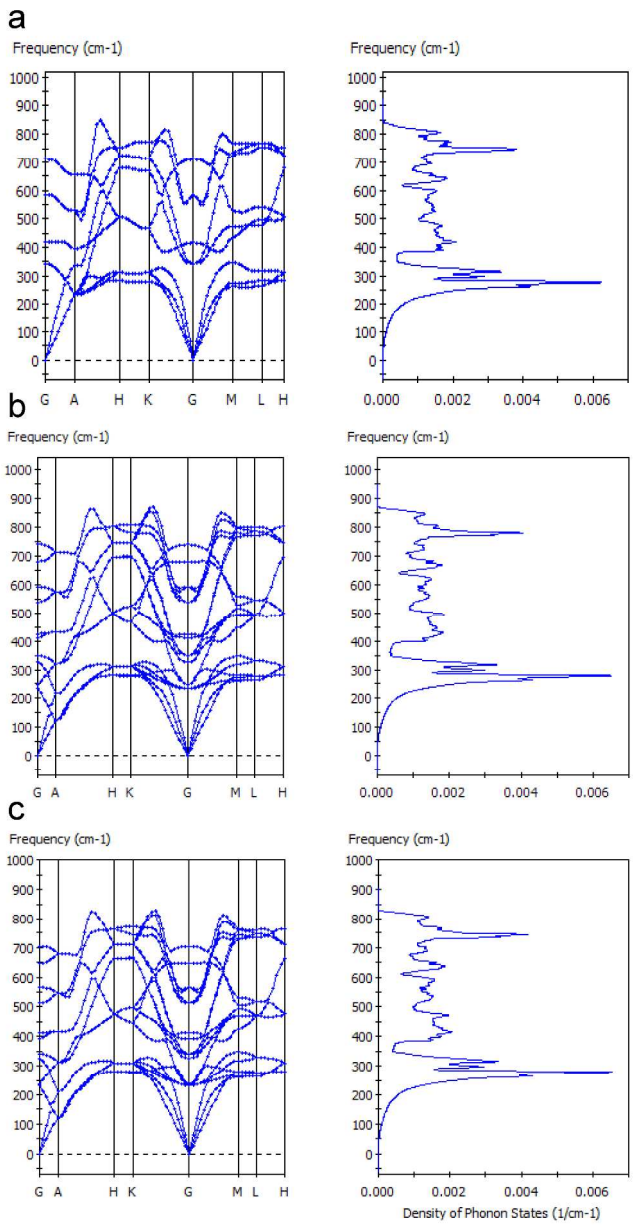

Fig. 1 Calculated PD of MgB_2 using linear response with k = 0.02 A^{-1} for: (a) space group P6/mmm and natural abundance boron, (b) space group P63mc and isotope ^{10}B and (c) space group P63mc and isotope ^{11}B.

uncertainties related to determination of the origin as noted above, the slope of the linear plot appears to incorporate these uncertainties and provides a reasonable approximation to the lowest multiple frequency.

Figure 4 shows a similar calculation of quantized frequencies for AlB_2 using the same symmetry conditions as for MgB_2. The phonon frequencies used in Figure 4 are derived from DFT calculations as shown in Table 2. The trend line in Figure 4 is well correlated with calculated frequency modes and a slope that suggests a low energy mode at ~81.1 cm^{-1}.

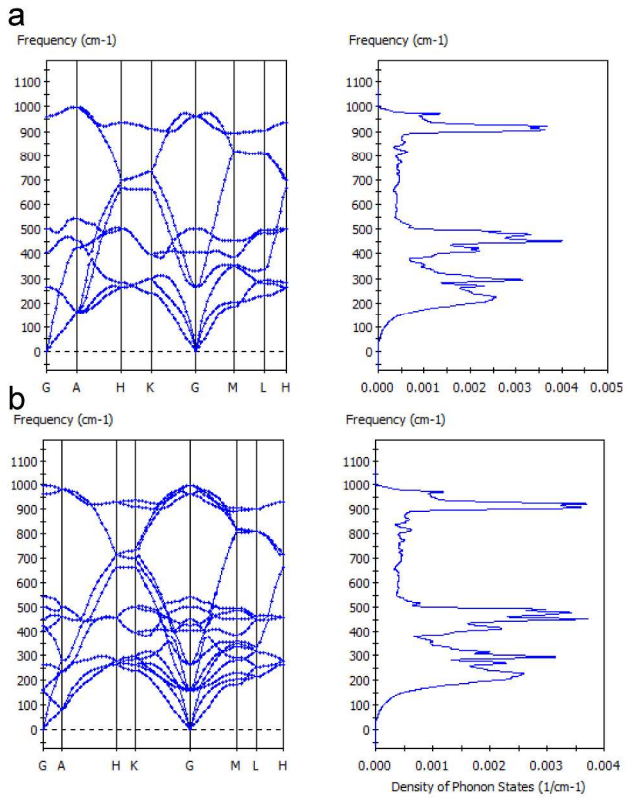

Fig. 2 Calculated PD of AlB_2 using linear response with k = 0.02 A^{-1} for: (a) space group P6/mmm and (b) space group P63mc. The PDs are for an energy cut-off value of 400 eV (see Table 2).

4. Discussion

Comparisons of the PDOS for both symmetry conditions (i.e. the conventional P6/mmm symmetry and the 2x super-lattice symmetry) on MgB_2 and on AlB_2, clearly show that the PDOS is insensitive to changes in imposed symmetry, even when additional frequencies occur. Note also that the phonon anomaly identified in earlier work[22] is present in the PDs for pure isotopic forms of MgB_2. This result indicates that the phonon anomaly does not originate from the natural mixture of isotopes which may be a potential source of local asymmetry.

4.1 Experimental

Our model calculations can be compared with existing experimental data collected on isotopic forms[17-19] as well as on natural abundance MgB_2[22, 23].

4.1.1 Phonon decay for MgB_2

A detailed Raman scattering study by Mialitsin et al.[23] on two MgB_2 singe crystals with particular emphasis on the $\mathbf{E_{2g}}$ phonon anharmonicity showed that two-phonon decay is a key mechanism that determines the broad linewidth of this mode. In these experiments, two-phonon scattering peaks at about 100 meV and 132 meV (i.e. 807 cm^{-1} and 1065 cm^{-1}, respectively) were observed in the 2.6 eV Raman response associated with

the $\mathbf{E_{2g}}$ mode at ~80 meV[23]. Mialitsin et al.[23] also show that the intensity of the ~80 meV (i.e. 645 cm^{-1}) Raman response is in resonance with the 2.6 eV band. In a footnote, Mialitsin et al.[23] indicate that the $\mathbf{E_{2g}}$ optical branch has a minimum at the **A** point at 66 meV (i.e. 532 cm^{-1}) resulting in one of the two phonon scattering peaks. This interpretation is consistent with our computational analysis of PD for MgB_2 which uses a super-lattice construct to interpret Raman and IR spectra[22]. Use of a 2x super-lattice in the *c*-direction requires **A** boundary modes with P6/mmm symmetry to be folded into centre zone modes of a lower symmetry structure[22].

In earlier work[22], we demonstrated that energy conservation through conversion of phonon energies by coherent relaxation is manifest as integer multiples of phonon energies reflected in the Raman and IR spectra of MgB_2. This mechanism is described in terms of the important $\mathbf{E_{2g}}$ mode which is strongly implicated in the BCS model for superconductivity in MgB_2[16]. This analysis of experimental data and *ab initio* calculations shows that major acoustic energies for a 2x super-lattice define a linear trend with integer multiples corresponding to allowed frequency modes[22] in MgB_2.

4.1.2 Isotopes of MgB_2

We now extend this analysis to the isotopic versions of MgB_2 given the model calculations shown above and earlier experimental results on isotopic forms. As noted earlier, the work by Simonelli et al.[17] measured a difference in Raman shift of about 30−35cm^{-1} for the two isotopic forms of MgB_2. In this work, our calculated values for the $\mathbf{E_{2g}}$ mode of the isotopic forms of MgB_2 differ by 27−28cm^{-1}. This Raman shift is similar to the experimentally measured values determined by Simonelli et al.[17]. The agreement is remarkably good, considering that model calculations are for absolute zero temperature conditions while the experimental data were collected at higher temperature. Furthermore, differences in calculated values are larger for higher value modes and reduce at lower frequencies; a trend consistent with the overall changes in slope shown in Figure 3.

For measurements of the superconducting gap, Bugovslaski et al.[42] report the values Δ = 7.2 meV and 6.5 meV for the 2-dim gap and the tunneling gap, respectively for MgB_2. These experimental values correspond to 2Δ = 14.4 meV = 116.1 cm^{-1} and 13 meV = 104.8 cm^{-1}, respectively. These values are close to our calculated acoustic frequency (233.4 cm^{-1}/2 = 116.7 cm^{-1}) and to the slopes of the linear trends shown in Figure 3. Furthermore, calculating $4k_BT_c$ where k_B is Boltzmann's constant and T_c is the transition temperature and converting to cm^{-1}, for T_c = 39.0 K and 40.2 K, (the experimental values for isotopic forms of MgB_2[15, 16]), we obtain $4k_BT_c$ = 108.6 cm^{-1} and 111.8 cm^{-1}. These values are similar to that determined by the slopes of the linear trends in Figure 3.

On the other hand, for AlB_2 the $\mathbf{E_{2g}}$ level[34] is at ~960 cm^{-1}. If this mode is essential for superconducting transport, a coherent decay path to the acoustic frequency cannot be established in

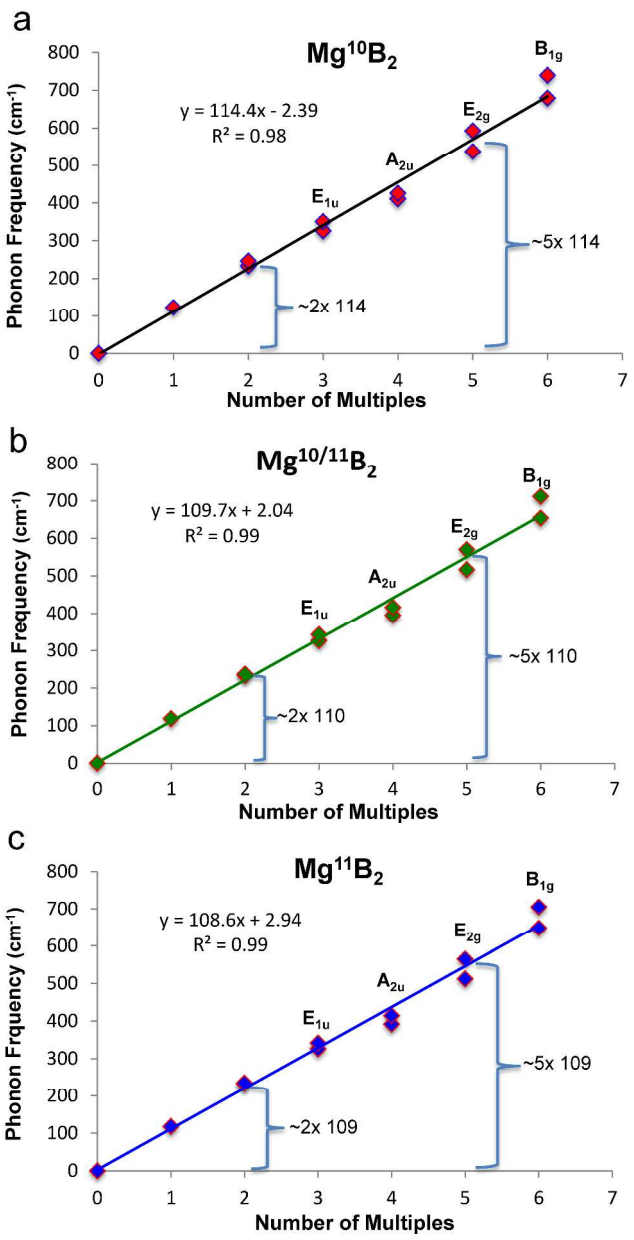

Fig. 3 Calculated phonon frequency plot of MgB_2 for space group P63mc with (a) isotope ^{10}B, (b) natural abundance and (c) isotope ^{11}B.

the same way that we have shown[22] for MgB_2. Figure 4 shows that a decay from the $\mathbf{E_{2g}}$ mode requires some other mechanism to effect conservation of energy transfer. In addition, the $\mathbf{E_{2g}}$ mode for AlB_2 may not be strongly coupled to electron or hole movement, as is the case for MgB_2[43-45]. For MgB_2, the important charge carriers are holes which strongly couple to the electronic band that is closely related to the generation of the $\mathbf{E_{2g}}$ mode in the PD[43-45].

For both compositions in this type structure, the correlation of vibration modes calculated for a super-lattice structure with experimental data is notable given the intrinsic sources of error in modelling programs and experimental methods. Some of

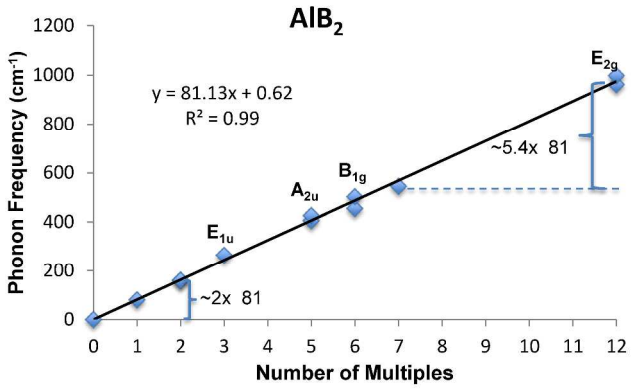

Fig. 4 Calculated phonon frequency plot for AlB_2 using the super-lattice space group P63mc.

these intrinsic sources of error are briefly described in section 4.2 below. In addition to choice of cut-off energy, improvements in DFT models that consider the dynamic nature of these systems would ensure greater precision with this type of analysis.

4.2 Intrinsic Sources of Error

The approach described above and in earlier work[22] provides an improved explanation for dynamic perturbations on the MgB_2 structure that are introduced by the phonons themselves and thus, result in a strongly-coupled electronic response[22]. While conventional DFT modelling can provide a guide to these phenomena, these computations are unable to represent dynamic interactions properly. Developments in time dependent-DFT (TD-DFT)[46-48], is, in principle, better equipped to deal with these phenomena and will provide greater insight to electron-phonon interactions when available.

Superconductors display magnetic flux expulsion through the Meissner effect which develops into a mixed vortex state as the field is increased. This phenomena implies that the superconducting material has dynamic magnetic interactions (although on average equal zero without external field) ready to produce the flux expulsion as soon as the field is increased. However, at the local level, this may generate forces that slightly modify a non-magnetic approach to phonon calculations.

Other sources of error include the current limitation that phonon calculations using the DFPT method in CASTEP cannot be implemented for spin-polarized structures[35-37]. This limitation makes it impossible to investigate potential contributions of magnetic effects with this computational method. An alternative method is use of the FD functional in CASTEP for spin-polarized situations. However, as shown in earlier work[22], the FD method is not as effective with Norm-conserving potentials as it is with ultrasoft potentials and can produce significant changes to the PD, particularly on the acoustic bands. This region is of particular interest for IE determinations and requires a consistent computational approach to effect useful comparison.

As mentioned in Section 3.0, geometry optimization results are insensitive to the isotopic composition. However, several examples with experimental evidence of isotopic effects on lattice parameters and thermal expansions have been reported[49-52]. For example, using a combination of zero point motion with anharmonicity, Hu et al.[50] obtained excellent agreement between theory and experiment for germanium. This likely source of intrinsic error indicates that the quantum mechanical DFT approach as currently implemented is oversimplified for determination of IE on lattice parameters. As a consequence, small errors in Coulomb and exchange energies can be expected in current computational models with subsequent errors in determination of phonon frequencies.

The original formalism of DFT calculations was designed for accurate determination of the ground state properties of a material, that is, at 0 K or low temperatures[22, 46]. Temperature effects are included in the calculation of specific properties by use of various modifiers. However, it is arguable whether the accuracy of calculation with these modifiers remains at the same level as the original quantum mechanical approach.

Phonon modes at any temperature above 0 K display a certain experimental full-width-at-half-maximum (FWHM). Thus, for phonon interactions, involving excitation and/or decay between modes, the separation between energy levels is relevant. Consideration of FWHM is an additional source of intrinsic error as it is well known from Raman and IR studies that the FWHM varies for different vibration modes. Between the appropriate choice of curve fitting routine (e.g. Lorentzian or Gaussian) and the influence of temperature, additional errors in the determination of mode separations may arise.

5. Conclusions

Integer multiple frequencies of the lowest energy vibration calculated using DFT for the isotopic forms of MgB_2 is consistent with experimental and predicted data on the IE for this compound. Use of a 2x super-lattice with reduced symmetry to calculate phonon modes, suggests that isotopic forms of MgB_2 follow a trend consistent with the IE. Thus, the important $\mathbf{E_{2g}}$ high energy mode may undergo coherent acoustic phonon decay while remaining within the set of integer modes. Integer multiples of acoustic energy equivalent to the lowest energy in the super-lattice structure can be interpreted[22] in terms of the superconducting gap for MgB_2. Minor variations between calculated and experimental values can be attributed to current limitations in software models that implement the DFT as well as intrinsic sources of error.

Acknowledgements

Financial assistance from QUT is gratefully acknowledged. Assistance with the High Performance Computing (HPC)

facilities from Ashley Wright, Adam Siliato and Mark Barry is also gratefully acknowledged.

Notes and references

* email: jose.alarco@qut.edu.au

[a] Institute for Future Environments

[b] Science and Engineering Faculty

Queensland University of Technology, 2 George St.,

Brisbane, QLD Australia 4001.

*corresponding author

See DOI: 10.1039/b000000x/

1. H. Fröhlich, *Physical Review*, 1950, 79, 845-856.
2. H. Fröhlich, *Proceedings of the Physical Society. Section A*, 1950, 63, 778.
3. J. Hirsch, *Physica Scripta*, 2011, 84, 045705.
4. E. Maxwell, *Physical Review*, 1950, 78, 477.
5. C. Reynolds, B. Serin and L. Nesbitt, *Physical Review*, 1951, 84, 691.
6. X. Huang, *arXiv preprint arXiv:1102.1467*, 2011.
7. J. Bardeen, L. N. Cooper and J. R. Schrieffer, *Phys. Rev.*, 1957, 108, 1175-1204.
8. J. R. Schrieffer, *Theory of Superconductivity*, Advanced Book Program, Westview, 1999.
9. M. Tinkham, *Introduction to Superconductivity*, Second edition, Dover Publications, Inc., 1996.
10. X.-J. Chen, V. V. Struzhkin, Z. Wu, H.-Q. Lin, R. J. Hemley and H.-k. Mao, *Proceedings of the National Academy of Sciences*, 2007, 104, 3732-3735.
11. G.-m. Zhao, H. Keller and K. Conder, *Journal of Physics: Condensed Matter*, 2001, 13, R569.
12. A. Mourachkine, *Room-temperature superconductivity*, Cambridge Int Science Publishing, 2004.
13. M. A. Malik and B. A. Malik, *American Journal of Condensed Matter Physics*, 2012, 2, 67-72.
14. A. Knigavko and F. Marsiglio, *Physical Review B*, 2001, 64, 172513.
15. S. Bud'Ko, G. Lapertot, C. Petrovic, C. Cunningham, N. Anderson and P. Canfield, *Physical Review Letters*, 2001, 86, 1877.
16. D. Hinks, H. Claus and J. Jorgensen, *Nature*, 2001, 411, 457-460.
17. L. Simonelli, V. Palmisano, M. Fratini, M. Filippi, P. Parisiades, D. Lampakis, E. Liarokapis and A. Bianconi, *Physical Review B*, 2009, 80, 014520.
18. J. W. Quilty, *Physica C*, 2003, 385, 264-272.
19. X. K. Chen, M. J. Konstantinovic´, J. C. Irwin, D. D. Lawrie and J. P. Franck, *Phys. Rev. Lett.*, 2001, 87, 157002-157001-157004.
20. A. Q. R. Baron, H. Uchiyama, Y. Tanaka, S. Tsutsui, D. Ishikawa, S. Lee, R. Heid, K.-P. Bohnen, S. Tajima and T. Ishikawa, *Phys. Rev. Lett.*, 2004, 92, 197004-197001-197004.
21. S. Tajima, T. Masui, J. Quilty, S. Lee, A. Yamamoto and A. Yamanaka, *Physica C*, 2003, 388-389, 103-104.
22. J. A. Alarco, A. Chou, P. C. Talbot and I. D. R. Mackinnon, *Physical Chemistry Chemical Physics*, 2014, DOI: 10.1039/C4CP03449J
23. A. Mialitsin, B. Dennis, N. Zhigadlo, J. Karpinski and G. Blumberg, *Physical Review B*, 2007, 75, 020509.
24. J. Nagamatsu, N. Nakagawa, T. Muranaka, Y. Zenitani and J. Akimitsu, *Nature*, 2001, 410, 63-64.
25. J. D. Jorgensen, D. G. Hinks and S. Short, *Phys. Rev. B*, 2001, 63, 224522-224521-224525.
26. S. Lee, H. Mori, T. Masui, Y. Eltsev, A. Yamamoto and S. Tajima, *Jour. Physical Society Japan*, 2001, 70, 2255-2258.
27. K.-P. Bohnen, R. Heid and B. Renker, *Phys. Rev. Lett.*, 2001, 86, 5771-5774.
28. L. Boeri, G. B. Bachelet, E. Cappelluti and L. Pietronero, *Physical Review B*, 2002, 65, 214501.
29. S. Souma, T. Sato, T. Takahashi, N. Kimura and H. Aoki, *Journal of electron spectroscopy and related phenomena*, 2005, 144, 545-547.
30. A. Q. R. Baron, H. Uchiyama, S. Tsutsui, Y. Tanaka, D. Ishikawa, J. P. Sutter, S. Lee, S. Tajima, R. Heid and K.-P. Bohnen, *Physica C*, 2007, 456, 83-91.
31. E. Deligoz, K. Colakoglu, H. Ozisik and Y. O. Ciftci, Lattice Dynamical Properties of AlB_2 Compound, http:\\www.ef.aksaray.edu.tr/fizik/edeligoz/16_2_2010_138.pdf.
32. J. Nakamura, S.-y. Nasubida, E. Kabasawa, H. Yamazaki, N. Yamada, K. Kuroki, M. Watanabe, T. Oguchi, S. Lee and A. Yamamoto, *Physical Review B*, 2003, 68, 064515.
33. Z. Xiao-Lin, L. Ke, C. Xiang-Rong and Z. Jun, *Chinese Physics*, 2006, 15, 3014.
34. I. Loa, K. Kunc, K. Syassen and P. Bouvier, *Physical Review B*, 2002, 66, 134101.
35. Accelrys, Materials Studio CASTEP Online Help: "Predicting the thermodynamic properties of germanium", http://www.tcm.phy.cam.ac.uk/castep/documentation/WebHelp/extfile/castep_tuts/html/castep_thermo_tut.htm#s4.
36. Accelrys, Materials Studio CASTEP Online Help: "Requesting vibrational properties", http://www.tcm.phy.cam.ac.uk/castep/documentation/WebHelp/html/taskcastepreqvibprops.htm.
37. Accelrys, Materials Studio CASTEP Online Help: "Calculating phonon spectra for ferromagnetic iron", http://www.tcm.phy.cam.ac.uk/castep/documentation/WebHelp/extfile/castep_tuts/html/castep_fdphonons_tut.htm.
38. K. Refson, Phonons and related calculations using CASTEP. Chapter 2: Running phonon calculations. , http://www.tcm.phy.cam.ac.uk/castep/Phonons_Guide/Castep_Phononsch2.html.
39. M. Born and K. Huang, *Dynamical Theory of Crystal Lattices Oxford Classic Texts in the Physical Sciences*, Clarendon Press, Oxford, 1988.
40. M. Fujimoto, *Thermodynamics of Crystalline States*, Springer, 2013.
41. J. A. Alarco, P. C. Talbot and I. D. R. Mackinnon, *Modeling and Numerical Simulation of Material Science*, 2014, 4, 53-69.
42. Y. Bugoslavsky, Y. Miyoshi, G. Perkins, A. Berenov, Z. Lockman, J. MacManus-Driscoll, L. Cohen, A. Caplin, H. Zhai and M. Paranthaman, *Superconductor Science and Technology*, 2002, 15, 526.
43. J. Kortus, I. I. Mazin, K. D. Belashchenko, V. P. Antropov and L. L. Boyer, *Phys. Rev. Lett.*, 2001, 86, 4656-4659.
44. J. M. An and W. E. Pickett, *Phys. Rev. Lett.*, 2001, 86, 4366-4369.
45. J. Kortus, http://www.physik.tu-freiberg.de/~kortus/kortus-research.html.
46. R. M. Dreizler and E. Engel, *Density functional theory*, Springer, 2011.
47. M. Marques and E. Gross, *Annu. Rev. Phys. Chem.*, 2004, 55, 427-455.
48. A. Soba, E. A. Bea, G. Houzeaux, H. Calmet and J. M. Cela, *Computer Physics Communications*, 2012, 183, 2581-2588.
49. V. Ozhogin, N. Babushkina, L. Belova, A. Zhernov, E. Haller and K. Itoh, *Journal of Experimental and Theoretical Physics*, 1999, 88, 135-137.
50. M. Hu, H. Sinn, A. Alatas, W. Sturhahn, E. Alp, H.-C. Wille, Y. V. Shvyd'ko, J. Sutter, J. Bandaru and E. Haller, *Physical Review B*, 2003, 67, 113306.
51. D. Gabunia, O. Tsagareishvili, L. Chkhartishvili and L. Gabunia, presented in part at the Journal of Physics: Conference Series, 2009.
52. L. S. Chkhartishvili, D. L. Gabuniya and O. A. Tsagareishvili, *Powder Metallurgy and Metal Ceramics*, 2008, 47, 616-621.